Article

Effect of Pyrolysis Temperature during Valorization of Date Stones on Physiochemical Properties of Activated Carbon and Its Catalytic Activity for the Oxidation of Cycloalkenes

Hamed M. Alshammari [1],* and Nadir Abbas [2]

1   Chemistry Department, Faculty of Science, University of Ha'il, P.O. Box 2440, Ha'il 81451, Saudi Arabia
2   Department of Chemical Engineering, College of Engineering, University of Ha'il, Ha'il 81441, Saudi Arabia; n.abbas@uoh.edu.sa
*   Correspondence: h.alshammari@uoh.edu.sa

Abstract: This study presents findings on the chemical synthesis of activated carbon from Saudi dates and its structural, chemical, and catalytic properties. Dates are among the top biowaste materials in the Kingdom of Saudi Arabia, and efforts are underway to utilize this resource. A chemical pyrolysis method was used to synthesize activated carbon from date stones. Synthesized activated carbon was calcined at different temperatures of 400, 500, 600, and 700 °C, and the impact of calcination temperature on the properties of activated carbon was investigated. For this purpose, contemporary characterization tools, namely, XRD, Raman spectroscopy, FTIR, SEM, TEM, TGA, DSC, and XPS, were employed. Results are discussed and compared with associated studies. Finally, the catalytic activity of gold-deposited activated carbon for the oxidation of cycloalkenes was evaluated, and it was found that the calcination temperature has a linear positive relationship with the catalytic activity.

Keywords: biomass; valorization; activated carbon; pyrolysis; Raman spectroscopy; date stones

1. Introduction

The synthesis of functional materials, such as catalysts, from biowaste is gaining importance due to increasing concern about the environmental impacts of major raw material consumption and due to the growing popularity of biowaste utilization. Biological waste, especially food byproducts, is disposed of and left for the environment to consume. However, recently with the world focusing more than ever on the preservation of our natural habitat, all relevant policy, engineering, chemical, and material handling aspects are being researched to minimize the environmental footprint of progress. Rice husk, corn cob, orange peel, bagasse, coconut husk, and tamarind seeds are just a few among many examples of biowaste being used for various valuable purposes [1–6].

Researchers are finding ways to use a variety of biowaste materials, including palm shell, grape stalk, bamboo, coconut shell, olive mill, almond shell, walnut shell, durian shell, banana empty fruit bunch, corn cob, sugar cane, and rice husk, to make activated carbon [7]. This biowaste-synthesized activated carbon has been found to be useful in applications such as hydrometallurgy, catalysis, energy-storing materials, fuel cells, batteries, electrode materials, construction materials, pharmacy, and beyond [4,6–8]. Studies have also investigated various procedures for synthesizing these materials and their effects. The effects of chemical activation, physical activation, impregnation ratio, temperature, and activating agents have all been the subject of recent studies [7,9,10]. Detailed and varying analysis of the morphology and porosity of activated carbon synthesized from various biowaste sources has confirmed that the type of raw material and conditions of synthesis can greatly impact the key performance properties of activated carbon [7,11,12]. It is therefore vital to discover novel biowaste-based raw materials and study the effects of various changing synthesis conditions on their properties.

In the context of Saudi Arabia, dates have been an important staple food for many centuries. Saudi Arabia is the second largest date producer in the world, behind only Egypt. According to the official website of the Ministry of Environment, Water and Agriculture of Saudi Arabia (accessed on 25 May 2021), Saudi Arabia accounts for 17% of global date production, and the annual production of dates is more than 1.5 million tons. With a much smaller population than Egypt, it is expected that a large quantity of dates is wasted every year. To address this potential, a number of researchers have been working to find possible options. Mansour et al. showed that brilliant green dye can be removed from wastewater by using date pit carbon [13]. Mouni et al. made use of date stone-synthesized activated carbon for the removal of lead and zinc ions from water [14]. Melliti et al. used date stones to prepare a material that can act as a tylosin antibiotic scavenger [15]. These examples show that date biowaste can be utilized as an effective source for various chemical purposes.

For the synthesis of activated carbon from dates, several strategies have been presented. We investigated the synthesis of activated carbon from date stones in this study, and we explored the catalytic properties of the synthesized activated carbon. We calcined the material at different temperatures and studied the effect of calcination. We had some interesting findings, which are discussed and compared with previous studies. Activated carbon structures were loaded with gold nanoparticles by the sol immobilization method. The purpose of adding these gold nanoparticles was to exploit the excellent catalytic abilities of Au catalytic cycles, which have the ability to oxidatively transform the in situ made bonds [16]. Naturally, while choosing a complimentary metal for our catalysts, gold emerged as a suitable choice because of its unique properties in activating unsaturated carbon entities by an electrophilic process [17–19].

2. Materials and Methods

2.1. Materials

Date stones, as a dried residual waste, were collected from the local area in Ha'il city, Saudi Arabia. Then, the stones were washed several times with deionized water, dried, and finally crushed into course-to-fine powder before use. Polyvinyl alcohol (PVA) used in this study was manufactured by Sigma-Aldrich (St. Louis, MO, USA, 1 wt.%, 80% hydrolyzed, Mw = 10,000). Sigma-Aldrich was also the manufacturer of $NaBH_4$ and phosphoric acid used in our experiments. $HAuCl_4 \cdot 3H_2O$ (Johnson Matthey, London, UK, 0.062 M, equivalent to 10 mg of Au) and $PdCL_2$ used during the sol immobilization process were purchased from Johnson Matthey.

2.1.1. Preparation of Activated Carbon (AC)

The preparation of activated carbon (AC) materials was achieved by a chemical activation method using phosphoric acid. Typically, 10 g of crushed date stones was mixed individually with phosphoric acid solutions by stirring at 85 °C, maintained for 3 h. After this step, to start the process of dehydration in the samples, we allowed an overnight drying of slurry at 110 °C. Then, pyrolysis was carried out at various temperatures for 1 h, at 400, 500, 600, and 700 °C (10 °C/min), in a flow of N_2 gas (150 mL/min) in a furnace tube. The resultant activated carbon was washed with plenty of distilled water until the filtrate reached neutral pH. In the last step, the AC material was left to dry in a drying oven at 110 °C and weighed.

2.1.2. Preparation of Au/AC Catalyst

The 1% Au catalysts were prepared by the sol immobilization method. As a standard, each 1% Au/Ac catalyst was prepared as follows: polyvinyl alcohol (PVA) was added to an aqueous solution of $HAuCl_4$-$3H_2O$, and then this solution was stirred robustly (PVA/Au (w/w) = 0.65) for around 15 min. Then, 0.1 M of freshly prepared $NaBH_4$ was added to the existing mixture, which created a dark brown solution. The pH of this mixture was maintained at 1 by addition of sulfuric acid, and the stirring of the mixture continued for

30 min. Active carbon (AC) (0.99 g) was also added at this stage to the mixture. After one further hour of stirring this slurry, a solid catalyst was obtained through filtration, washed with 2 L of distilled water, and then left to dry overnight at 110 °C.

2.1.3. Catalyst Testing

Oxidation of cycloalkenes (cyclohexene and cyclooctene) was performed in a glass reactor, which was essentially a round-bottomed glass flask. First, 0.02 g of catalyst was added to the reaction mixture, which contained 3 mL of cycloalkene and was continuously stirred. Solvents were not used but a small amount of TBHP (0.002×10^{-3} mol, 70% in H_2O) was injected to act as a radical initiator. The reaction mixture was then stirred at 50 °C and 1 bar of O_2. Stirring speed was maintained at 1000 rpm.

A sample was withdrawn from the reaction mixture at regular intervals, as presented in the results, and analyzed by gas chromatography (3800 GC Agilent technologies, Palo Alto, Santa Clara, CA, USA), which encompassed a detector based on the principle of flame ionization.

2.2. Characterizations

X-ray diffraction (XRD) analysis was carried out to study and confirm the structural characteristics of synthesized activated carbon. XRD analysis was carried out by using Shimadzu diffractometer equipment (XRD-6000). With the increased focus on carbon-based materials such as graphene, Raman spectroscopy has emerged as the major analysis technique to study the state of carbon in complex structures. An Enwave Optronics ProRaman-L spectrometer was used to record the Raman spectra presented in this study with a 532 nm laser for excitation. FTIR data were taken from analysis on FT-IR Nicolet 6700 by Thermos Scientific, Oklahama, OK, USA. Analysis of material surfaces by X-ray photoelectron spectroscopy (XPS) was carried out on a K-ALPHA (Thermo Fisher Scientific, Waltham, MA, USA) instrument. Thermal analysis was carried out using an NETZSCH STA 409 C/CD instrument in a helium atmosphere. Scanning electron microscopy images were obtained to study the morphology of prepared samples by Zeiss FESEM Ultra 60 (Oberkochen, Germany). High-resolution transmission electron microscopy (HRTEM) images were acquired at 200 kV using a JEOL model JEM 2100F TEM instrument (Tokyo, Japan).

3. Results and Discussion

We used contemporary analysis techniques to understand the true nature of prepared activated carbon-based catalysts. Herein, the results and discussion of these analyses are presented systematically.

3.1. X-ray Diffraction Analysis

To evaluate the effects of calcination temperature, various activated carbon samples annealed at different calcination temperatures were analyzed by XRD. Figure 1 shows that all the diffractograms exhibit the typical activated carbon pattern with a strong peak at 25° and a weak peak at around 45° values of 2θ [20]. These peaks can be attributed to carbon planes of 002 and 101, and this is in conformity with the hexagonal structure of graphitic carbonaceous materials [10,20]. Notably, there are small yet important differences in the intensity of the major peak around 25°. With the increase in calcination temperature, a sharper peak is apparent in the XRD trends of activated carbon synthesized in this study. The size of the graphite crystallites was calculated by the Debye–Scherrer equation, which showed that crystallite size is less than 1 nm for all activated carbon samples. We believe that in many other cases, the Debye–Scherrer equation does not represent the accurate size of crystallites.

It is well-known that the complete wall of the material we are studying, i.e., activated carbon, is made up of graphite crystallites. If the crystallite size increases with the rise in calcination temperature, we can expect a more packed structure with narrowing or

ordering of internal structures. Meanwhile, smaller crystalline materials in this case would generally have greater surface areas. Activated carbon is made up of fine particles and has a porous structure.
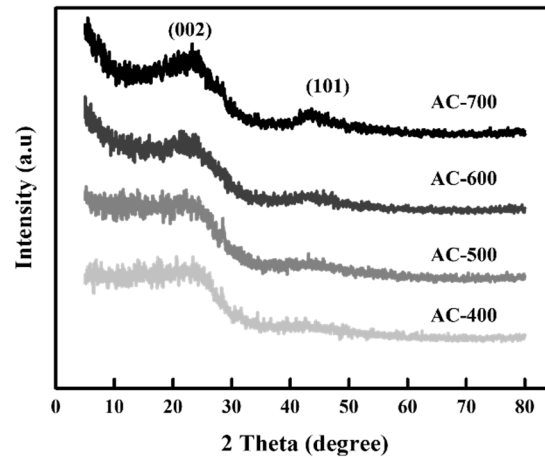

Figure 1. XRD patterns obtained for AC-400, AC-500, AC-600, and AC-700, as indicated.

3.2. Spectroscopic Analyses

The Raman spectroscopy technique can obtain data about the rotational energy or molecular vibration of the substance under study, identify it, and provide information about its nature. Raman spectra of AC-400, AC500, AC-600, and AC-700 are shown in Figure 2. The distinctive D and G bands of carbon materials around 1340 cm^{-1} and 1600 cm^{-1} are visible in the spectra of all samples [21]. This observation confirms the formation of activated carbon from date stones. It is also well-known that graphitic materials have a large number of peaks in Raman spectra, and hence a number of small peaks between 0 and 1000 cm^{-1} is no surprise [9]. It can be inferred from these observations that activated carbon has been successfully synthesized and its structure remains intact irrespective of the change in calcination temperature.
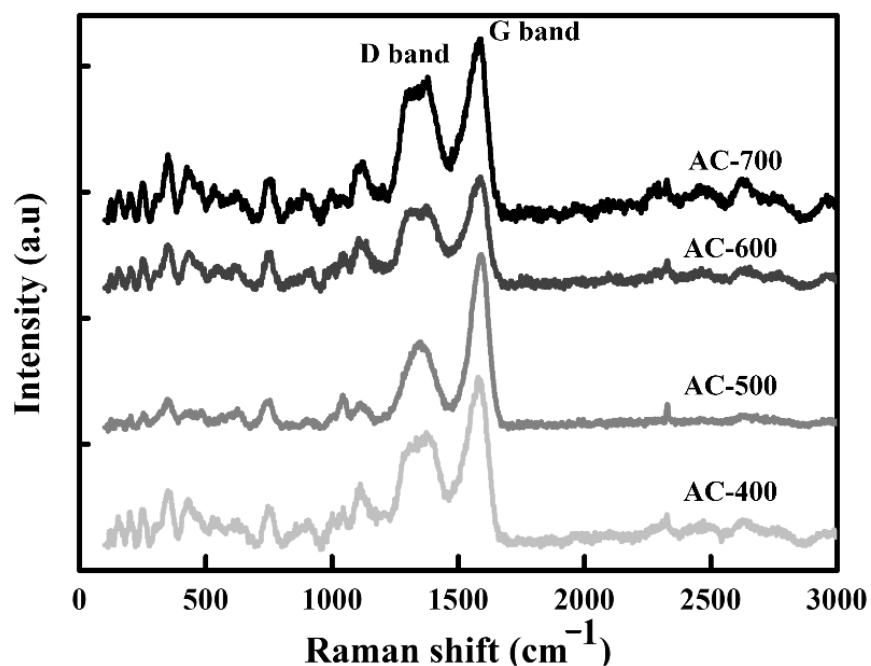

Figure 2. Raman spectra obtained for AC-400, AC-500, AC-600, and AC-700, as indicated.

Figure 3 displays the FTIR spectra of activated carbon synthesized from date stones via pyrolysis and calcined at various temperatures. Transmittance of AC-400, AC-500, AC-600, and AC-700 at various wavenumbers is shown in the Figure 3. The distinctive feature of these spectra is the sharp bands between 1000 and 1700 cm^{-1}, which are thought to be occurring because of C–O and COOH groups due to oxidation of activated carbon [22,23]. The peaks at 2854 and 2924 cm^{-1} might be due to the presence of both C-H aromatic stretching vibrations and –CH$_2$– bridges [24]. As we compare the spectra of activated carbon calcined at lower temperatures of 400–500 °C with those of samples calcined at 600–700 °C, we notice two important trends: firstly, the gradual decrease in overall transmittance, and secondly, shifting of the major peak from 1580 to 1450 cm^{-1}. Peaks around the region of 1580 cm^{-1} in activated carbon samples have been attributed to pyrrolic, pyridonic, or pyridinic structures [25]. Some other studies on activated carbon have attributed this peak to stretching vibrations in C–C, which are a component of the aromatic ring [26]. The latter seems more plausible for the current study. A strong absorption at 1010 cm^{-1} shows the presence of C–O stretching vibrations [26]. Another weak band near 870 cm^{-1} might be due to amine groups.
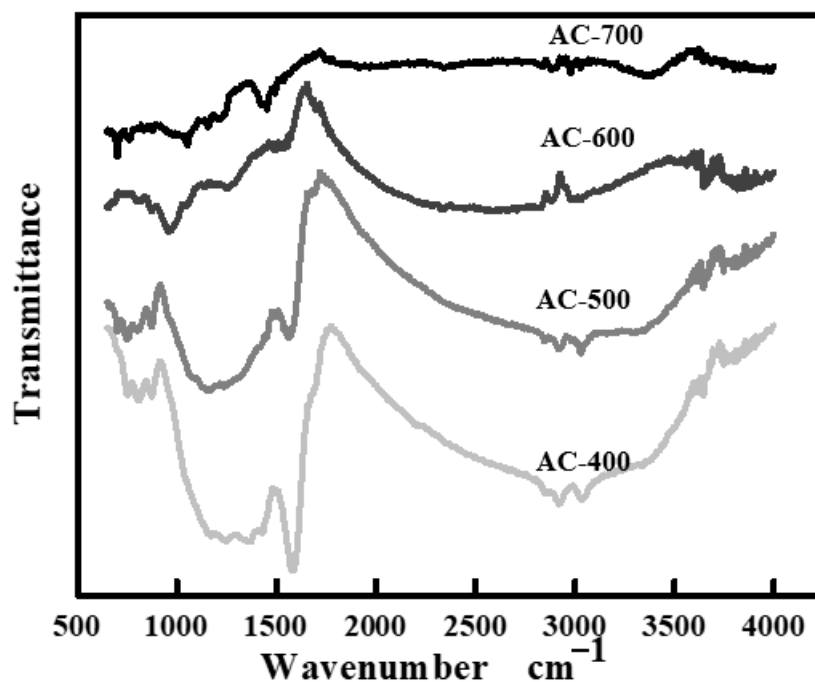

Figure 3. FT-IR spectra obtained for AC-400, AC-500, AC-600, and AC-700, as indicated.

X-ray photoelectron spectroscopy (XPS) is a surface analysis technique that can give us important information about the chemical nature of samples. The chemical state and electronic environment of our samples were further analyzed by XPS, and results are presented in Figure 4. The presence of elemental gold is ascertained by a double peak occurring at 84.4 and 88.1 eV; these peaks correspond to Au$_{4f7/2}$ and Au$_{4f5/2}$, respectively [27,28]. Similarly, the typical peaks of activated carbon-based materials for C1s at 286 eV and O1s at 533 eV are also a prominent feature of the XPS survey spectrum, which confirms the presence of these elements on the surface of the catalyst. This is predictable for activated carbon materials and is merely a confirmation of the presence of both activated carbon and gold material on the surface.
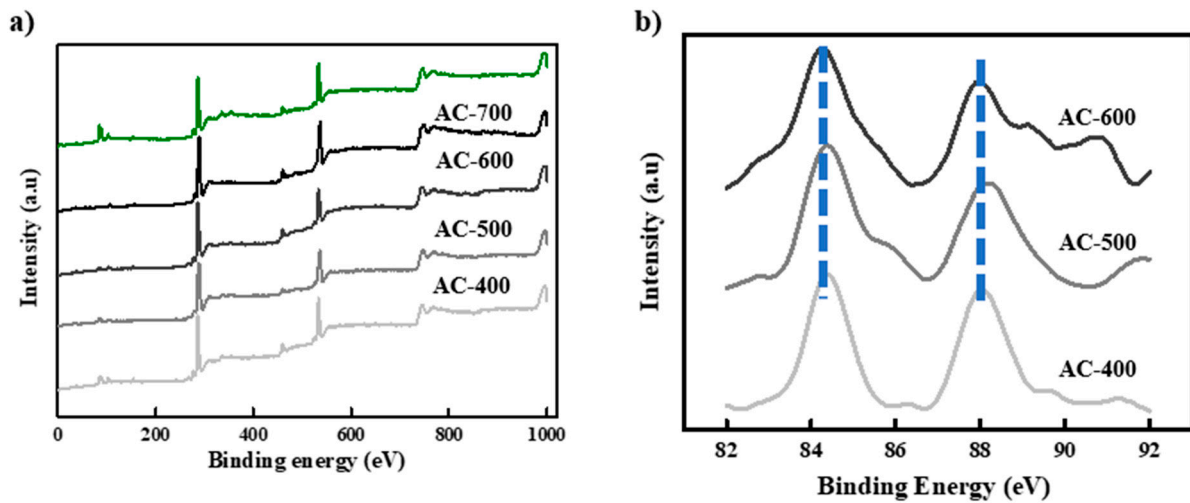
Figure 4. (**a**) XPS survey spectrum of various activated carbon-based catalysts; (**b**) high-resolution XPS spectra of Au.

3.3. Thermal Analyses (TGA-DTG and DSC)

A thermal stability study was carried out using thermogravimetric analysis (TGA) and derivative thermogravimetry (DTG). TGA/DTG curves of a representative sample, AC-400, are shown in Figure 5. The shape of the TGA curve depends on the thermal behavior of carbon materials. It is clear from the trend that single-step decomposition occurs initially, followed by small DTG decomposition peaks. This initial major weight loss can be attributed to the removal of physically adsorbed water between 50 and 170 °C. Final weight loss was found to be 14.1%, 6.4%, and 2.4% for AC-400, AC-500, and AC-600 respectively.
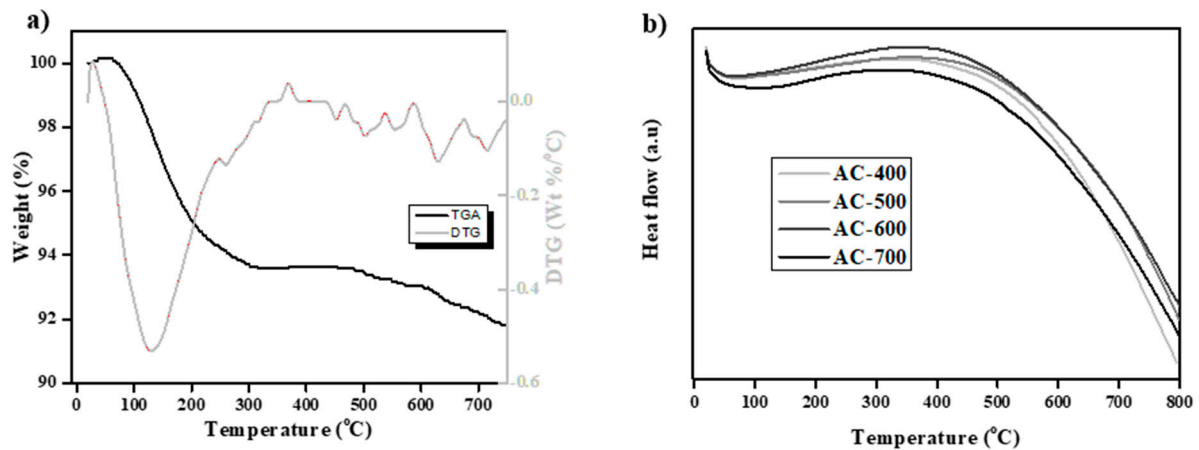

Figure 5. (**a**) TGA (black curve) and DTG (gray curve) analyses obtained for AC-700 whilst heating to 800 °C (10 °C/min); (**b**) DSC curves of AC-400, AC-500, AC-600, and AC-700 samples.

3.4. Electron Microscopy Studies

Scanning electron microscopy (SEM) is a powerful tool to look at the morphology of materials. Figure 6 shows the SEM images of AC-400, AC-500, AC-600, and AC-700 samples. The images are at two different resolutions to compare the samples on various scales. It is important to evaluate the effects of different calcination temperatures. Left side images of Figure 6 show that the surface of all samples, regardless of calcination temperature, is concealed by various sub-micrometer-sized particles, and a number of distinct cleavages are present on the surface. The pyrolysis at various calcination temperatures causes

insignificant changes in the morphology of AC samples, with slight changes such as removal of some particles from the surface and erosion of some cleavages. Furthermore, it can be deduced from these SEM images that the availability of a number of micropore structures in these activated carbon materials makes them an excellent host for reactant interaction in any kind of chemical reaction.
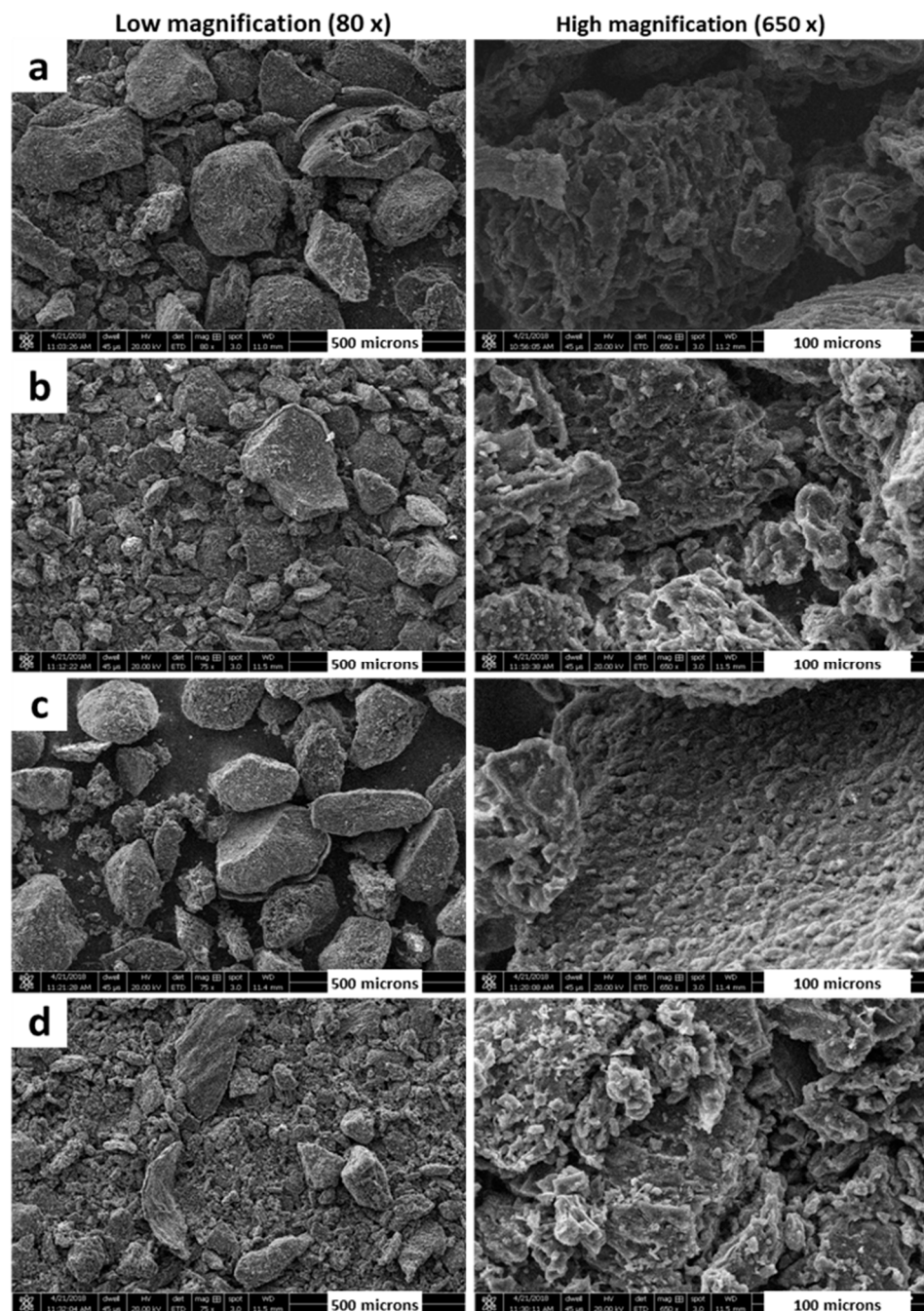

Figure 6. SEM micrographs obtained for (**a**) AC-400, (**b**) AC-500, (**c**) AC-600, and (**d**) AC-700 samples. Scale bars are 500 and 100 μm at low (left, 80×) and high (right, 650×) magnifications, respectively.

To further our investigations on the distribution of gold particles on the surface of activated carbon and crystallinity, we took transmission electron microscope images of gold-coated activated carbon Au/AC samples. Figure 7 shows the TEM images at various magnifications of various Au/AC samples. Figure 7a,b show the distribution of gold

nanoparticles on the surface of activated carbon. It is evident that the distribution is even in both samples. It seems that both AC-400 and AC-600 have interacted and hosted Au nanoparticles in a similar manner. High-resolution TEM images taken of the Au/AC-700 samples are presented in Figure 7c,d. Figure 7c shows that most of the gold nanoparticles are small, with 3–5 nm diameter, and only a few agglomerated particles are seen. Figure 7d shows the lattice fringe spacing of gold. It is found that the lattice fringe spacing is 0.236 nm, which corresponds to the (111) facet of gold crystal planes [29]. Furthermore, we tried to estimate the distribution of particle sizes through TEM images, and we found that for all samples more than 80% of Au particles are less than 5 nm in size.
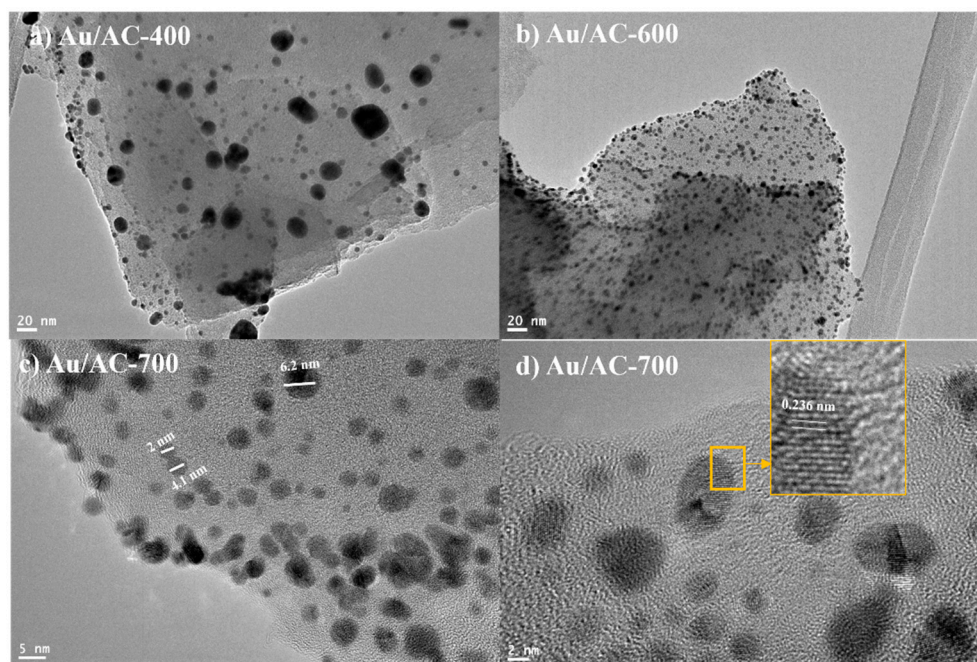

Figure 7. TEM images of Au/AC catalysts. (**a**) Au/AC-400, (**b**) Au/AC-600, (**c**) high-magnification image showing size of gold nanoparticles, (**d**) HRTEM image of gold nanoparticle shown in inset.

3.5. Catalytic Conversion of Cycloalkene

　　The fabricated sol-immobilized 1% Au/AC catalysts, calcined at different temperatures, were examined for the oxidation of cyclooctene (Table 1) and oxidation of cyclohexene (Table 2). There were two major trends in the readings for conversion; the first one, which is typical, was the increase in conversion with increase in reaction time, and the second one was the positive influence of increasing calcination temperature on the conversion. Tables 1 and 2 show the selectivity towards the epoxide. There are clear indications of a bimodal distribution in the selectivity from the data over the time studied. Our previous work showed that selectivity to epoxide was low for the smaller ring sizes (C5–C7), but the selectivity increased significantly for the larger ring sizes of C8 and C12 rings [18]. At the conversion levels achieved in this work, the data show that selectivity towards the epoxide product was steady over the time studied for all activated carbon-based catalysts. We also carried out a reaction with a catalyst that was calcined at 800 °C, but it showed similar conversion to that of Au/AC-700. We believe that activated carbon structures were fully developed at 700 °C as evident from XRD patterns. These robust support structures could have contributed to the performance in catalysis of cycloalkenes. A blank experiment without catalyst addition showed less than 0.1% conversion, which hints at the positive role of the catalyst in these reaction conditions. Table 2 shows the results of the reaction in the oxidation of cyclohexene.

Table 1. Oxidation of cyclooctene using 1% Au/AC catalyst.

Catalyst	Time (h)	Conversion	Selectivity to Epoxide
Au/AC-400	2	0.2	72
	4	0.3	77
	6	0.5	75
Au/AC-500	2	0.3	75
	4	0.38	80
	6	0.5	82
Au/AC-600	2	0.6	87
	4	1.2	88
	6	1.8	86
Au/AC-700	2	0.9	85
	4	1.5	85
	6	2.1	88

Reaction conditions: 3 mL of cyclooctene, 0.02 g catalyst, TBHP (0.002×10^{-3} mol), 50 °C, 1 bar of O_2, and stirring at 1000 rpm.

Table 2. Oxidation of cyclohexene using 1% Au/AC catalyst.

Catalyst	Time (h)	Conversion	Selectivity		
			Epoxide	Cyclohexenone	Cyclohexenol
Au/AC-400	2	0.41	5.3	50.1	41.3
	4	0.47	6	49.8	40
	6	0.6	5.8	51	40.6
Au/AC-500	2	0.4	5.1	51.2	42.1
	4	0.6	5.6	50.4	41
	6	0.68	5.7	50.3	40.9
Au/AC-600	2	0.9	5.9	49.8	41
	4	1.6	6.3	49.8	41.3
	6	2.3	6.4	50.2	40.8
Au/AC-700	2	1.3	6.3	49.7	39.8
	4	2	6.5	50	39.9
	6	3.1	6.7	49.8	40.1

Reaction conditions: 3 mL of cyclohexene, 0.02 g catalyst, TBHP (0.002×10^{-3} mol), 50 °C, 1 bar of O_2, and stirring at 1000 rpm.

4. Conclusions

Activated carbon was effectively synthesized from date stones, and its catalytic activity was determined. Contemporary characterization techniques were adopted to ascertain the nature of activated carbon. XRD confirmed the presence of a hexagonal structure, which is typical of such carbon-based materials, hence confirming the synthesis of activated carbon from the date stones. Raman spectroscopy also confirmed the presence of carbon bands pertaining to activated carbon. The chemical environment of activated carbon materials synthesized from date stones was further analyzed by XPS and FTIR, which demonstrated the intact chemical structure of AC and AC/Au catalysts. SEM and TEM showed excellent porous structure, morphology, and particle size characteristics. It was found that gold nanoparticles were on average less than 5 nm wide. These are essential traits of catalysts. Hence, the catalytic studies also showed significant activity in the oxidation of cycloalkenes. It was noted that catalytic activity increases with the increase in the calcination temperature for activated carbon structures synthesized from date stones. Conversion increased from 0.5% to 2.1% and selectivity to epoxide increased from 75% to 88% when the calcination temperature for activated carbon synthesis was raised from 400 to 700 °C.

References

1. Mopoung, S.; Moonsri, P.; Palas, W.; Khumpai, S. Characterization and Properties of Activated Carbon Prepared from Tamarind Seeds by KOH Activation for Fe(III) Adsorption from Aqueous Solution. *Sci. World J.* **2015**, *2015*, 1–9. [CrossRef] [PubMed]
2. El-Sayed, G.O.; Yehia, M.M.; Asaad, A.A. Assessment of activated carbon prepared from corncob by chemical activation with phosphoric acid. *Water Resour. Ind.* **2014**, *7–8*, 66–75. [CrossRef]
3. Hu, J.; Luo, J.; Zhu, Z.; Chen, B.; Ye, X.; Zhu, P.; Zhang, B. Multi-Scale Biosurfactant Production by *Bacillus subtilis* Using Tuna Fish Waste as Substrate. *Catalysts* **2021**, *11*, 456. [CrossRef]
4. Abbas, N.; Khalid, H.R.; Ban, G.; Kim, H.T.; Lee, H. Silica aerogel derived from rice husk: An aggregate replacer for lightweight and thermally insulating cement-based composites. *Constr. Build. Mater.* **2019**, *195*, 312–322. [CrossRef]
5. Tovar, A.K.; Godínez, L.A.; Espejel, F.; Ramírez-Zamora, R.-M.; Robles, I. Optimization of the integral valorization process for orange peel waste using a design of experiments approach: Production of high-quality pectin and activated carbon. *Waste Manag.* **2019**, *85*, 202–213. [CrossRef] [PubMed]
6. Han, J.; Zhang, L.; Zhao, B.; Qin, L.; Wang, Y.; Xing, F. The N-doped activated carbon derived from sugarcane bagasse for CO2 adsorption. *Ind. Crop. Prod.* **2019**, *128*, 290–297. [CrossRef]
7. Yahya, M.A.; Al-Qodah, Z.; Ngah, C.Z. Agricultural bio-waste materials as potential sustainable precursors used for activated carbon production: A review. *Renew. Sustain. Energy Rev.* **2015**, *46*, 218–235. [CrossRef]
8. Manoochehri, M.; Khorsand, A.; Hashemi, E. Role of modified activated carbon by H 3 PO 4 or K 2 CO 3 from natural adsorbent for removal of Pb(II) from aqueous solutions. *Carbon Lett.* **2012**, *13*, 115–120. [CrossRef]
9. Junior, M.A.A.; Matsushima, J.T.; Rezende, M.C.; Gonçalves, E.S.; Marcuzzo, J.S.; Baldan, M.R. Production and Characterization of Activated Carbon Fiber from Textile PAN Fiber. *J. Aerosp. Technol. Manag.* **2017**, *9*, 423–430. [CrossRef]
10. Sonal, S.; Prakash, P.; Mishra, B.K.; Nayak, G.C. Synthesis, characterization and sorption studies of a zirconium(iv) impregnated highly functionalized mesoporous activated carbons. *RSC Adv.* **2020**, *10*, 13783–13798. [CrossRef]
11. Ioannidou, O.; Zabaniotou, A. Agricultural residues as precursors for activated carbon production—A review. *Renew. Sustain. Energy Rev.* **2007**, *11*, 1966–2005. [CrossRef]
12. Giraldo, L.; Moreno-Piraján, J.C. Synthesis of Activated Carbon Mesoporous from Coffee Waste and Its Application in Adsorption Zinc and Mercury Ions from Aqueous Solution. *E-J. Chem.* **2012**, *9*, 938–948. [CrossRef]
13. Mansour, R.A.E.-G.; Simeda, M.G.; Zaatout, A.A. Removal of brilliant green dye from synthetic wastewater under batch mode using chemically activated date pit carbon. *RSC Adv.* **2021**, *11*, 7851–7861. [CrossRef]
14. Mouni, L.; Merabet, D.; Bouzaza, A.; Belkhiri, L. Removal of Pb^{2+} and Zn^{2+} from the aqueous solutions by activated carbon prepared fromDates stone. *Desalin. Water Treat.* **2010**, *16*, 66–73. [CrossRef]
15. Melliti, A.; Srivastava, V.; Kheriji, J.; Sillanpää, M.; Hamrouni, B. Date Palm Fiber as a novel precursor for porous activated carbon: Optimization, characterization and its application as Tylosin antibiotic scavenger from aqueous solution. *Surf. Interfaces* **2021**, *24*, 101047. [CrossRef]
16. Zhang, G.; Cui, L.; Wang, Y.; Zhang, L. Homogeneous Gold-Catalyzed Oxidative Carboheterofunctionalization of Alkenes. *J. Am. Chem. Soc.* **2010**, *132*, 1474–1475. [CrossRef]
17. Iglesias, A.; Muñiz, K. Oxidative Interception of the Hydroamination Pathway: A Gold-Catalyzed Diamination of Alkenes. *Chem. A Eur. J.* **2009**, *15*, 10563–10569. [CrossRef]
18. Alshammari, H.; Miedziak, P.J.; Knight, D.W.; Willock, D.J.; Hutchings, G.J. The effect of ring size on the selective oxidation of cycloalkenes using supported metal catalysts. *Catal. Sci. Technol.* **2013**, *3*, 1531–1539. [CrossRef]
19. Alshammari, H.; Miedziak, P.J.; Davies, T.E.; Willock, D.J.; Knight, D.W.; Hutchings, G.J. Initiator-free hydrocarbon oxidation using supported gold nanoparticles. *Catal. Sci. Technol.* **2014**, *4*, 908–911. [CrossRef]
20. Xie, Z.; Guan, W.; Ji, F.; Song, Z.; Zhao, Y. Production of Biologically Activated Carbon from Orange Peel and Landfill Leachate Subsequent Treatment Technology. *J. Chem.* **2014**, *2014*, 1–9. [CrossRef]
21. Shu, J.; Cheng, S.; Xia, H.; Zhang, L.; Peng, J.; Li, C.; Zhang, S. Copper loaded on activated carbon as an efficient adsorbent for removal of methylene blue. *RSC Adv.* **2017**, *7*, 14395–14405. [CrossRef]
22. Şencan, A.; Kılıç, M. Investigation of the Changes in Surface Area and FT-IR Spectra of Activated Carbons Obtained from Hazelnut Shells by Physicochemical Treatment Methods. *J. Chem.* **2015**, *2015*, 1–8. [CrossRef]

23. Zolfaghari, G.; Esmaili-Sari, A.; Younesi, H.; Baydokhti, R.R. Surface modification of ordered nanoporous carbons CMK-3 via a chemical oxidation approach and its application in removal of lead pollution from water. In Proceedings of the 2nd International Conference on Environmental Science and Technology, IPCBEE, Singapore, 26–28 February 2011; Volume 6, pp. 174–178.

24. Moyo, M.; Nyamhere, G.; Sebata, E.; Guyo, U. Kinetic and equilibrium modelling of lead sorption from aqueous solution by activated carbon from goat dung. *Desalin. Water Treat.* **2014**, *57*, 765–775. [CrossRef]

25. Jia, Y.F.; Xiao, A.B.; Thomas, K.M. Adsorption of Metal Ions on Nitrogen Surface Functional Groups in Activated Carbons. *Langmuir* **2002**, *18*, 470–478. [CrossRef]

26. Mohammad, S.; Ahmed, S.; Badawi, A.; El-Desouki, D. Activated Carbon Derived from Egyptian Banana Peels for Removal of Cadmium from Water. *J. Appl. Life Sci. Int.* **2015**, *3*, 77–88. [CrossRef] [PubMed]

27. Jiang, P.; Xie, S.; Yao, J.; He, S.; Zhang, H.; Shi, D.; Pang, S.; Gao, H. Two-dimensional self-organization of 1-nonanethiol-capped gold nanoparticles. *Chin. Sci. Bull.* **2001**, *46*, 996–998. [CrossRef]

28. Fujita, A.; Ryuto, H.; Matsumoto, Y.; Takeuchi, M.; Takaoka, G.H. Growth behavior of gold nanoparticles synthesized in unsaturated fatty acids by vacuum evaporation methods. *Phys. Chem. Chem. Phys.* **2016**, *18*, 5464–5470. [CrossRef]

29. Biao, L.; Tan, S.; Meng, Q.; Gao, J.; Zhang, X.; Liu, Z.; Fu, Y. Green Synthesis, Characterization and Application of Proanthocyanidins-Functionalized Gold Nanoparticles. *Nanomaterials* **2018**, *8*, 53. [CrossRef]